Mitral Valve Imaging with CT: Relationship with Transcatheter Mitral Valve Interventions

Jonathan R. Weir-McCall, MBBS, PhD • Philipp Blanke, MD • Christopher Naoum, MBBS, PhD • Victoria Delgado, MD, PhD • Jeroen J. Bax, MD, PhD • Jonathon Leipsic, MD, FRCPC

From the UBC Department of Medical Imaging, Centre for Heart Valve Innovation, St Paul's Hospital and University of British Columbia, 1081 Burrard St, Vancouver, BC, Canada V6Z 1Y6 (J.R.W.M., P.B., J.L.); Department of Cardiology, Concord Hospital, The University of Sydney, Sydney, Australia (C.N.); and Department of Cardiology, Leiden University Medical Center, Leiden, the Netherlands (V.D., J.J.B.). Received November 30, 2017; revision requested January 9, 2018; revision received February 6; accepted February 6. Supported in part by a generous unrestricted grant from the Arnold and Anita Silber Foundation. **Address correspondence to** P.B. (e-mail: *phil.blanke@gmail.com)*.

Study supported by Arnold and Anita Silber Foundation and the Syd and Joanne Belzberg Foundation.

Conflicts of interest are listed at the end of this article.

Radiology 2018; 288:638–655 • https://doi.org/10.1148/radiol.2018172758 • Content codes: CA CH CT

The role of noninvasive imaging to help guide transcatheter aortic valvular interventions is well established and has grown with the advances in the procedure. With the rapid development of new transcatheter mitral valve interventions there is both an opportunity and a challenge for noninvasive imaging to grow understanding of mitral valve anatomy and disease, help with patient selection, and improve downstream clinical outcomes. This review will discuss the role of both echocardiography and multidetector CT in the diagnosis of mitral regurgitation, as well as grading of its severity and defining its etiology. Additionally, new concepts including measurements pertaining to mitral annular sizing, segmentation of mitral annular calcium, prediction of neo-left ventricular out flow tract obstruction, hybrid or fusion multidetector CT/echocardiographic imaging, and CT-based fluoroscopic guidance will be discussed.

Online SA-CME • *See www.rsna.org/learning-center-ry*

Learning Objectives:

After reading the article and taking the test, the reader will be able to:

- Identify the anatomy of the mitral valve as it relates to structural intervention
- Recognize the complementary role of echocardiography and CT for assessment and characterization of mitral valve disease
- Describe the findings from CT that are useful for informing and guiding management choice and interventional approach

Accreditation and Designation Statement

The RSNA is accredited by the Accreditation Council for Continuing Medical Education (ACCME) to provide continuing medical education for physicians. The RSNA designates this journal-based SA-CME activity for a maximum of 1.0 *AMA PRA Category 1 Credit™*. Physicians should claim only the credit commensurate with the extent of their participation in the activity.

Disclosure Statement

The ACCME requires that the RSNA, as an accredited provider of CME, obtain signed disclosure statements from the authors, editors, and reviewers for this activity. For this journal-based CME activity, author disclosures are listed at the end of this article.

Mitral valve disease is the most common valvular heart disorder, affecting almost 10% of people over 75 years of age (1). Mitral regurgitation is the most common disorder of the mitral valve and can be divided into primary (structural or degenerative abnormality of the mitral valve) or secondary (disease of the left ventricle [LV] interfering with the function of the mitral valve apparatus) mitral regurgitation (2). Both primary and secondary mitral regurgitations are associated with significant morbidity, including an increased risk for heart failure and arrhythmia and increased mortality (3,4). Mitral stenosis is less common than mitral regurgitation, affecting 0.2% of the population (1). It is most commonly caused by rheumatic disease, but heavy calcification of the mitral annulus with involvement of the leaflets can also produce significant stenosis, particularly in the elderly population (5). Options for intervention in mitral valve disease have advanced significantly in the past decade (2). With the rapid development of percutaneous mitral valve therapies, radiologists and cardiologists will need to advance their understanding of mitral valve anatomy and function to meet the growing clinical need for informative periprocedural imaging. The mitral valve is a much more complex structure than the aortic valve as it cannot be considered in isolation. Rather, it requires an understanding of the valve and the subvalvular mitral apparatus, as well as their anatomic relationships and role in function, all of which vary across mitral valve pathology (6). Historically, the role of noninvasive imaging for the assessment of the mitral valve has been largely limited to the assessment of hemodynamic disturbances through the use of echocardiography (7–9). With the introduction of percutaneous annuloplasty devices, transcatheter mitral valve (TMV) repair and TMV replacement (TMVR), noninvasive imaging is playing an ever-greater role in the anatomic and functional evaluation (10–13). Importantly, echocardiography is no longer the only test needed for mitral evaluation. CT is playing an increasing role in annular assessment, landing zone characterization, defining relevant relationships with adjacent structures, and even in the adjudication and grading of mitral valvular stenosis and regurgitation (14). In this review, we focus on the essential elements and recent advancements of mitral valve

Abbreviations

LV= left ventricle, LVOT = LV outflow tract, MAC = mitral annular calcification, TAVR = transcatheter aortic valve replacement, TMV = tanscatheter mitral valve, TMVR = TMV replacement, 3D = three-dimensional

Summary

Rapid advancements in transcatheter mitral valve procedures have driven an increasing demand on noninvasive imaging to help assist in evaluation and procedural planning, with echocardiography and CT playing complementary roles in preprocedural work-up.

Essentials

- Evidence supporting transcatheter mitral valve intervention is growing.
- Echocardiography and CT play a complementary role in the work-up for transcatheter mitral valve insertion.
- A saddle-shaped annulus makes measurement challenging; however, the CT ability for volumetric anatomic review is well suited for this.

assessment in the context of TMV interventions and the complementary roles of echocardiography and multidetector CT.

Essential Anatomy of the Mitral Valve

The mitral valve anatomy has proven to be more challenging for evaluation than the aortic annulus. The aortic annulus is a vascular structure at the junction of the aorta and the LV defined by the crown-shaped insertion of the aortic valve cusps. The aortic annulus may be analyzed in an axial oblique imaging plane aligned so as to intersect the most basal hinge points of these three cusps. The mitral valve apparatus on the other hand comprises much more than a simple annular plane between the left atrium and LV. Rather, the mitral valve apparatus includes a fibrous annulus, chordae, and papillary muscles and their attachments, as well as the mitral valve leaflets (6,10,11,15) (Fig 1).

Annulus

The mitral annulus is a nonsymmetric fibrous structure with a three-dimensional (3D) saddle-shaped configuration. This consists of two horns, or peaks, separated by a nadir located in close approximation to the medial and lateral fibrous trigones (triangular-shaped fibrous structures at the inflection of the mitral annulus). The anterior horn of the mitral annulus proceeds in an upward fashion to the root of the aorta, where it is in fibrous continuity with the aortic valve–a key distinguishing feature of the anatomic LV. This continuity is known as the "aortomitral continuity" or the "intervalvular fibrosa." The aortomitral continuity is one of the most readily appreciable components of the fibrous endoskeleton of the heart on images (Fig 1, *B* and *D*). Due to its interposition between the mitral and aortic valves, it inherently encroaches upon the LV outflow tract (LVOT). This relationship is critical for consideration of anatomic suitability for TMVR (examined in more detail in the section LVOT Obstruction Assessment). In nondiseased state, the posterior horn is located at the junction of the atrial and ventricular myocardium and it is where the posterior mitral valve leaflet inserts (Fig 1, *B* and *D*). The fibrous trigones represent the anatomic junction between the anterior and posterior annulus and define the nadir of the saddle-shaped annulus; these are key structures in the assessment of the mitral valve as they can readily and reliably be identified on CT scans as focal areas of triangular thickening (Fig 1, *E*).

Leaflets

The mitral valve has two leaflets, the anterior mitral leaflet (AML) and the posterior mitral leaflet (PML), also referred to as the aortic and mural leaflets. Each leaflet has three scallops: A1–A3 anteriorly and P1–P3 posteriorly (Fig 1, *A* and *C*). Importantly, the mitral valve leaflets are unequal in size and shape. The AML occupies only one-third of the annular circumference, whereas the PML occupies the remaining two-thirds of the circumference and exhibits a narrower radial length. The coaptation zone, or line, describes a semilunar arc-like configuration, with the leaflets converging at the anterolateral and posteromedial commissures (Fig 1, *A*). These commissures lie approximately 5 mm centripetally to the annulus itself (2,6,15). It is well established that the scallops of the PML are more pronounced and clearly defined. The scallops of the AML are more poorly defined and are often unequal in size, with the middle scallop typically the largest. Given partial volume averaging and limited temporal resolution of CT, the distinct scallops of the mitral valve are not as well seen as on echocardiography. Some of this can be overcome through the use of minimum intensity projections to improve visualization of the thin low-attenuation leaflets in the contrast-enhanced cavity. By convention, the AML and PML are each subdivided into three equal components: A1, A2, A3 and P1, P2, P3 to designate the lateral, middle, and medial segments, respectively (Fig 2).

Subvalvular Apparatus

The subvalvular apparatus comprises the papillary muscles and chordae tendinae. The papillary muscles are named by convention based on their location and the commissures they relate to. The anterolateral and posteromedial papillary muscles give rise to the anterolateral and posteromedial commissures. While these are considered as two muscles, in reality each of these are themselves comprised of one to three muscular bundles. These typically arise from the apical and mid ventricle, extending basally to give rise to the fibrous string like chords of the chordae tendinae. These chords are highly variable in their number and configuration and extend down onto the mitral valve leaflets themselves both at the leaflet tips and in the mid leaflet body. Chordae can be distinguished on the basis of their leaflet insertion, with marginal or primary chords attached to the free edge of the leaflets and the basal or secondary chords inserting onto the central body of the anterior leaflet and broadly onto the posterior leaflet body. Finally, there are third-order chordae that are separate from the papillary muscles, instead extending directly from the ventricular wall to the base of the annulus and mural leaflet of the valve (6,12,15). While seemingly redundant and unnecessarily complex, this relationship between the mitral valve leaflets and papillary muscle chordal complex

is essential as it helps optimize functioning of both the mitral valve leaflets and the adjacent ventricle. Loss of these cords leads to loss of normal ventricular torsion, systolic thickening, and altered LV morphology (16,17).

State of Technology in TMV Intervention

There remains some ongoing debate as to whether mitral valve repair or replacement is the best strategy; however, current guidelines advocate that a repaired native mitral valve is preferred when possible (18,19).

This debate is more pronounced in the minimally invasive arena, where transcatheter procedures can tackle the issue of mitral regurgitation via repair or replacement. Current and new techniques for repair take different approaches to reduce MR: *(a)* fasten the two leaflets of the mitral valve together as seen with the MitraClip (Abbott, Abbott Park, Ill) system (20); *(b)* use individually adjustable clasps to place a spacer between the mitral valve leaflets as with the PASCAL (Edwards Lifesciences, Irvine, Calif) TMV repair system (21); *(c)* directly reduce annular dimensions through the use of implanted annular anchors, restoring the mitral leaflets to a more functional position as with the Cardioband (Edwards Lifesciences) mitral valve reconstruction system (22); or *(d)* indirectly reduce the annular dimension via a device inserted into the coronary sinus to improve coaptation of the native mitral leaflets as with the Carillon Mitral Contour System (Cardiac Dimensions, Kirkland, Wash) (23). Transcatheter repair techniques are more established than are transcatheter replacement systems, having been the first to be introduced clinically; however, over the past 3 years rapid development and introduction of TMVR devices has occurred, with eight such devices now under clinical evaluation (Fig 3) (16).

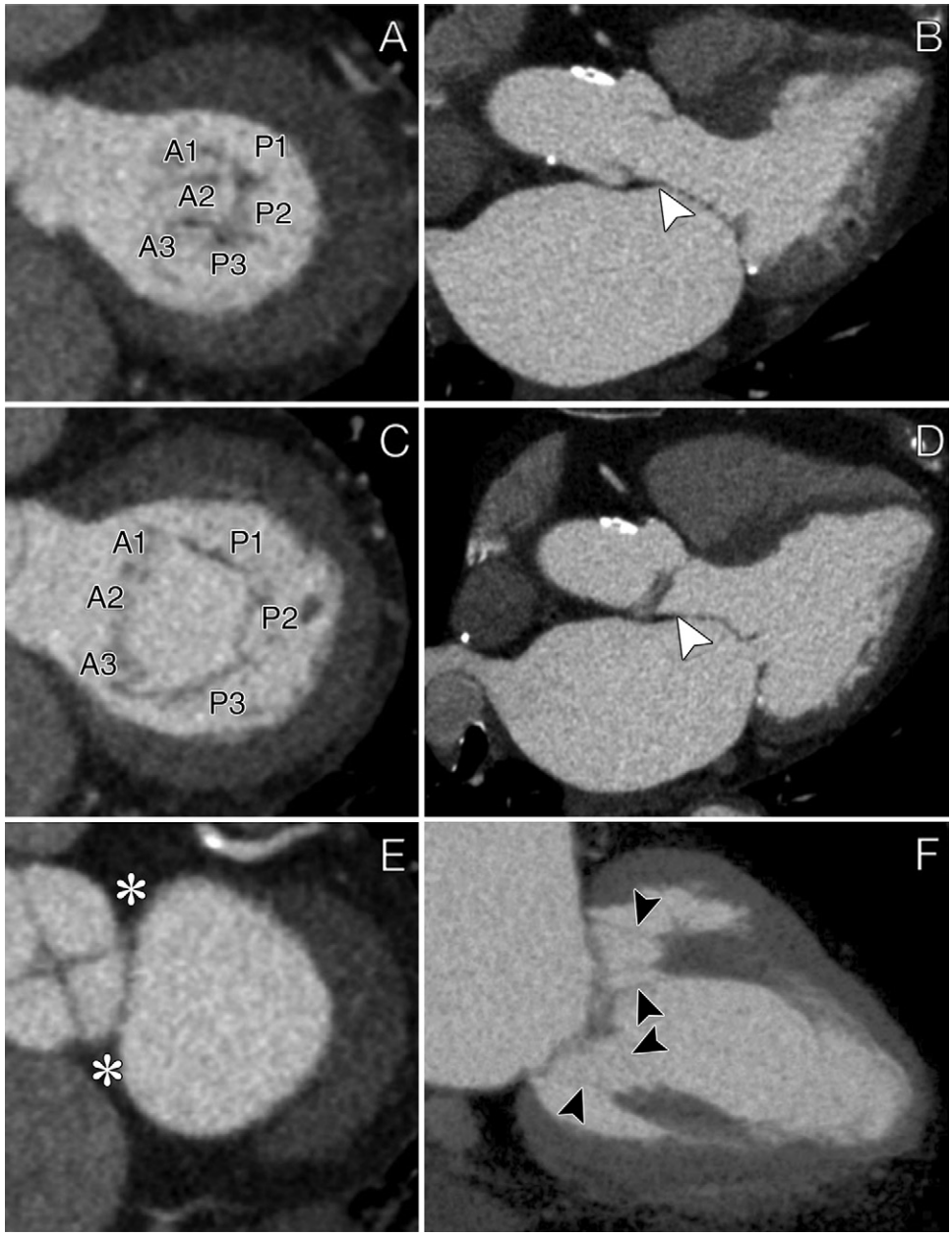

Figure 1: Anatomy of the mitral valve as demonstrated at CT. *A, B,* The mitral valve is closed at end systole. *C, D,* Images show the opened valve at end diastole, with the location of the three scallops of the anterior *(A1–A3)* and posterior *(P1–P3)* mitral valve leaflet; arrowhead (*B, D*) highlights the aortomitral continuity forming the anterior horn of the annulus remaining fixed in position throughout the cycle. *E,* Image shows mitral annulus and fibrous trigones (*). *F,* Minimum intensity projection at end systole highlights the complex fan-like radiation of fine tendinae running from the papillary muscles to the mitral leaflets (arrowheads).

High technical success rates have been reported with use of repair strategies, but these are commonly unable to eliminate mitral regurgitation entirely, with 57% of patients undergoing MitraClip and 45% of patients undergoing Cardioband procedures having significant residual mitral regurgitation at follow-up (22,24). The procedures are also somewhat reliant on the native valvular apparatus integrity to seat the device. Another limitation of these procedures is their inability to treat mitral valve stenosis or mitral bioprosthetic valve failure. That being said, repairing the mitral valve offers the benefit of more natural hemodynamic environment, no need for anticoagulation, and a favorable

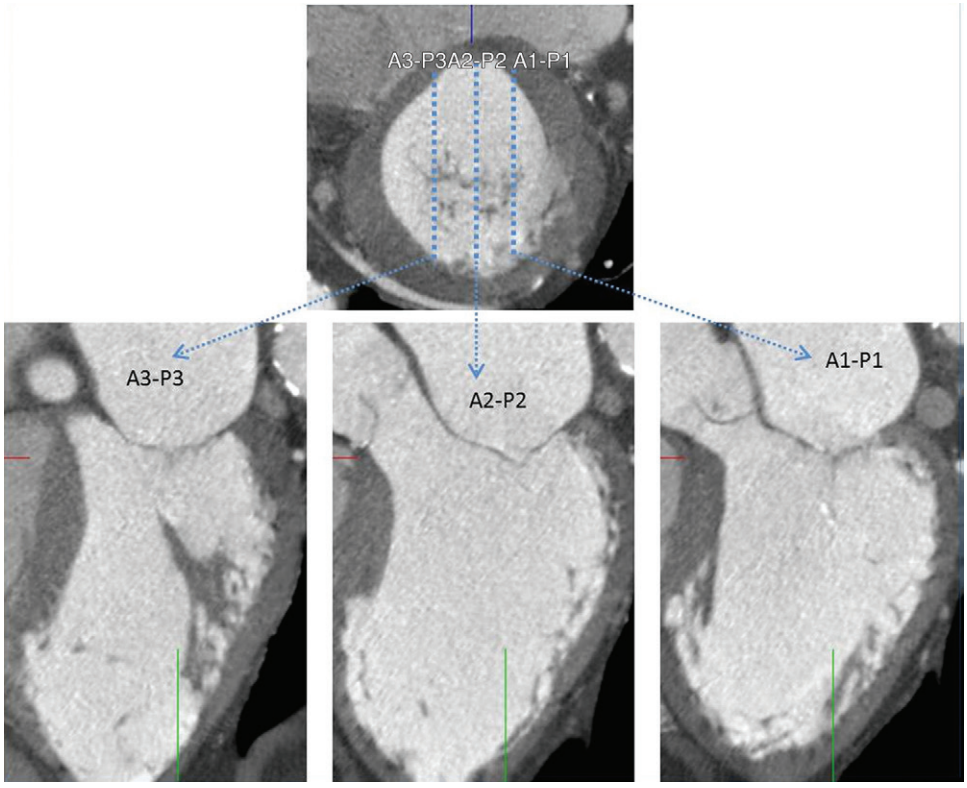

Figure 2: Assessment of mitral valve geometry with CT in a patient with secondary mitral regurgitation. From the reconstructed short-axis view of the mitral valve, the orthogonal plane can be set across the medial *(A3–P3)*, central *(A2–P2)*, and lateral *(A1–P1)* levels of the mitral valve to obtain the length, tenting height, and leaflet angles of the anterior and posterior mitral leaflets.

safety profile (25,26). TMVR, on the other hand, seeks to eradicate mitral regurgitation through the percutaneous replacement of the regurgitant mitral valve. Valve replacement offers the potential, depending on the design of the device, to treat a broader spectrum of mitral valvular disease but at present represents a much more complicated strategy with many anatomic limitations, particularly given the size of the valve that needs to be deployed (16).

The mitral valve offers further challenges that are not shared with the aortic valve (27). To start, transcatheter aortic valve replacement (TAVR) is performed for aortic stenosis and the pathophysiology of aortic stenosis is almost uniformly calcific aortosclerosis (27). Mitral regurgitation on the other hand results from a wide spectrum of pathologic conditions, ranging from regional and global LV dysfunction to degenerative valvular disease. In addition, the mitral annulus is a more complex anatomic structure with a nonplanar saddle-shaped configuration and extensive ventricular attachments and relationships. This complex anatomy leaves significant technical challenges that will need to be answered with numerous repair and replacement devices currently being tested taking a number of different approaches.

Imaging Assessment of the Mitral Valve

Imaging assessment of the mitral valve is essential in the work-up of mitral regurgitation. It is used for the identification of mitral regurgitation, quantification of its severity, characterization of its underlying cause, assessment of its suitability for structural intervention, and procedural planning. Echocardiography, CT, and MRI play a complementary role in this work-up, and the strengths of each should be utilized for the maximum benefit of the patient.

Quantification of Mitral Regurgitation

Echocardiography is the imaging technique of first choice in the evaluation of patients with mitral regurgitation since it provides comprehensive information on the regurgitation severity, its underlying mechanism, and the effect of volume overload on the cardiac chambers and pulmonary circulation. This information, along with clinical symptoms, determines the clinical treatment of patients with mitral regurgitation. In routine clinical practice, definition of severe mitral regurgitation is largely based on two-dimensional Doppler echocardiography. Qualitative parameters describe the mitral valve morphology and the characteristics of the regurgitant jet. Semiquantitative parameters reflect the degree of volume overload, and quantitative parameters estimate the effective regurgitant orifice area and regurgitant volume. Together with LV and atrial dimensions, these assessments form a multiparametric approach to grade mitral regurgitation (Table 1). These parameters are simple to obtain and permit an accurate estimate of the severity of the regurgitant lesion in the majority of patients (Fig 4). A discussion of the strengths and weaknesses of each of these is beyond the scope of the current review, but an excellent overview of these can be found in the review by Thavendiranathan et al (28).

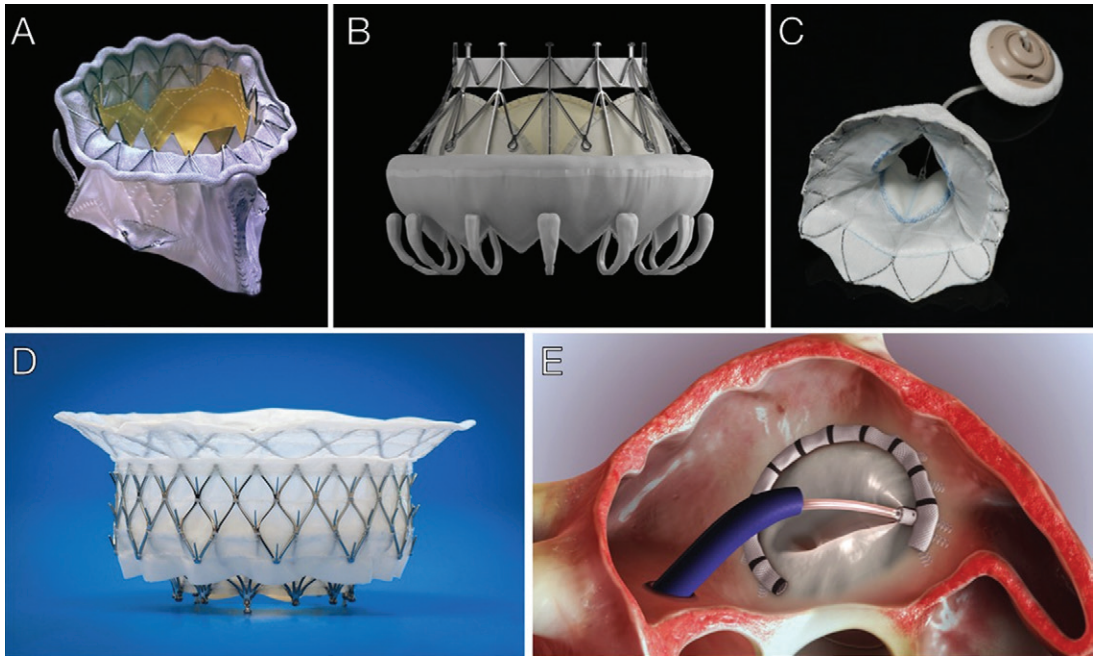

Figure 3: Examples of percutaneous mitral valve devices currently in use: *A,* Tiara (Neovasc, Richmond, BC, Canada), *B,* CardiAQ-Edwards Transcatheter Mitral Valve (Edwards Lifesciences, Irvine, Calif), *C,* Tendyne (Tendyne Holdings, Milosevic, Minn), *D,* Intrepid TMVR (Medtronic, Minneapolis, Minn), and, *E,* Cardioband Mitral Valve Reconstruction System (Edwards Lifesciences).

Regardless of whether the reader performs echocardiography himself or herself or not, it is essential to understand the parameters and the thresholds used for the diagnosis and grading of severe mitral regurgitation, which is a prerequisite for structural intervention. The most important of these and their respective thresholds for classification of severe mitral regurgitation are an effective regurgitant orifice area of 0.4 cm^2 or greater, regurgitant volume of 60 mL or greater, and regurgitant fraction of 50% or greater (7). However, eccentric regurgitant jets and/or multiple regurgitant jets can result in underestimation of the effective regurgitant orifice area and regurgitant volume based on two-dimensional proximal isovelocity surface area (29). Three-dimensional echocardiography and acquisition of full-volume color Doppler data permits a more accurate definition of the anatomic regurgitant orifice area (Fig 5). Use of these tools demonstrated better agreement for quantification of regurgitant volume with cardiac MRI than with two-dimensional echocardiography, with the latter tending to significantly underestimate the regurgitant volume (30–32).

Accurate measurement of the regurgitant orifice area is an important determinant in the estimation of the regurgitant volume. Where there is discordance between measures of mitral regurgitation severity or between symptom severity and mitral regurgitation severity, other cross-sectional techniques may aid in adjudication. MRI plays a key role in this regard. MRI can quantify mitral regurgitation in one of three ways: *(a)* Phase contrast sequences, which can be used to quantify aortic flow volume and cine sequences can quantify LV stroke volume. The difference between the aortic forward flow volume and LV stroke volume accurately calculates the mitral regurgitant volume, with a single study suggesting that this technique better predicts favorable LV remodeling following surgical intervention than do echocardiographic parameters of mitral regurgitation severity (33). *(b)* The difference between LV stroke volume and right ventricle stroke volume is equal to the regurgitant volume; however, this only holds true in the absence of shunts or other valvular regurgitation. *(c)* Direct quantification of the mitral regurgitation through the use of a transannular phase contrast sequence acquisition. The accuracy of this is significantly reduced in the presence of multiple regurgitant jets and underestimates regurgitation if the plane of acquisition is not truly perpendicular to the regurgitant jet (34).

Multidetector CT can also play a complementary role. As CT acquisition for valvular work-up typically involves full cycle acquisition, right ventricle and LV stroke volumes can be quantified with the regurgitant volume calculated from the stroke volume difference, with this correlating well with MRI (35). CT anatomic measures can also be used in conjunction with hemodynamic measures from transthoracic echocardiography to capitalize on the strengths of both. In a recent study of 73 patients with severe aortic stenosis and mitral regurgitation undergoing dynamic multidetector prior to TAVR, measurement of the anatomic regurgitant orifice area was feasible. By integrating dynamic CT with Doppler echocardiography data, the recalculated regurgitant volume reclassified 14% of patients from having nonsignificant to having significant mitral regurgitation (Fig 5) (36).

Mechanism of Mitral Regurgitation

As for the quantification of the severity of mitral regurgitation, echocardiography is key to diagnose the mechanism of mitral regurgitation. Primary mitral regurgitation is caused by

Table 1: Echocardiographic Criteria of Severe Mitral Regurgitation and Technical Advantages and Limitations

Parameter	Severe Mitral Regurgitation	Advantages	Limitations
Qualitative			
Mitral valve morphology	Flail leaflet/ruptured papillary muscle	Specific for severe mitral regurgitation	Other abnormalities are nonspecific for severe mitral regurgitation
Color flow mitral regurgitation jet	Large central jet or eccentric jet adhering, swirling, and reaching the posterior wall of the left atrium (coanda effect)	Simple, evaluates spatial orientation of the regurgitant jet and is good for screening	Inaccurate, particularly in eccentric regurgitant jets with coanda effect
Flow convergence zone	Large	Simple, flow convergence at 50 cm/sec indicates significant mitral regurgitation	Shape affected by aliasing velocity, noncircular regurgitant orifice, systolic changes in regurgitant flow
Continuous wave Doppler signal of the mitral regurgitation jet	Dense/triangular	Simple	Difficult to obtain in eccentric regurgitant jets
Semiquantitative			
Vena contracta width (mm)	≥7 (> 8 for biplane view)	Simple, relatively independent of hemodynamic factors, not affected by other valve leaks, can be used in eccentric jets	Not valid for multiple jets
Mitral inflow	E-wave dominant (≥ 1.2 m/sec)	Simple, specific for severe mitral regurgitation	Affected by left atrium pressure and atrial fibrillation
Pulmonary vein flow	Systolic flow reversal (more specific if > 1 pulmonary vein)	Simple	Affected by left atrium pressure and atrial fibrillation and left ventricle relaxation
VTI mitral/VTI aortic	>1.4	Simple	Affected by left atrium pressure and atrial fibrillation, left ventricle relaxation and aortic pressures
Quantitative, primary			
EROA (mm^2)	≥40	Not affected by etiology of mitral regurgitation, can be used in eccentric jets, quantitative estimates of lesion severity	PISA shape affected by aliasing velocity, noncircular regurgitant orifice, systolic changes in regurgitant flow
Regurgitant volume (mL)	≥60		Errors in PISA measurements are squared
Regurgitant fraction (%)	≥50		Not valid in multiple jets

Source.—Reference 7.

Note.—EROA = effective regurgitant orifice area, PISA = proximal isovelocity surface area, VTI = velocity time integral.

an anatomic abnormality or direct damage of the mitral leaflets, chordae, annulus, and papillary muscles. Secondary mitral regurgitation is caused by regional or global dysfunction and/or dilatation of the LV, causing tethering and restriction of the mitral leaflets and coaptation failure (Fig 6). Three-dimensional echocardiography provides en face views of the mitral valve resembling the surgical view and facilitates the communication between imagers, cardiac surgeons, and interventional cardiologists. In primary mitral regurgitation, 3D echocardiography permits accurate characterization and localization of the prolapsing scallops and has important implications in the evaluation of surgical and transcatheter ability to repair the mitral valve (11). The agreement between surgical exploration of the mitral valve and 3D transesophageal echocardiography is superior to two-dimensional transesophageal echocardiography, particularly in patients with complex lesions involving multiple mitral scallops, the anterior mitral leaflet, or the commissures (76% vs 47%, respectively) (37). In those who cannot undergo transoesophageal echocardiography, MRI has been demonstrated to have a high accuracy for the detection and localization of degenerative mitral valve disease (38). MRI can also provide useful information on the underlying etiology of functional mitral regurgitation, which can aid in guiding management strategies (34).

In secondary mitral regurgitation, several parameters of mitral valve and LV remodeling have been associated with high rates of mitral regurgitation recurrence after surgical repair (39). These measures include *(a)* mitral valve remodeling—coaptation distance or tenting height greater than 10 mm, tenting area greater than 2.5–3 cm^2, posteromedial regurgitant jets, and

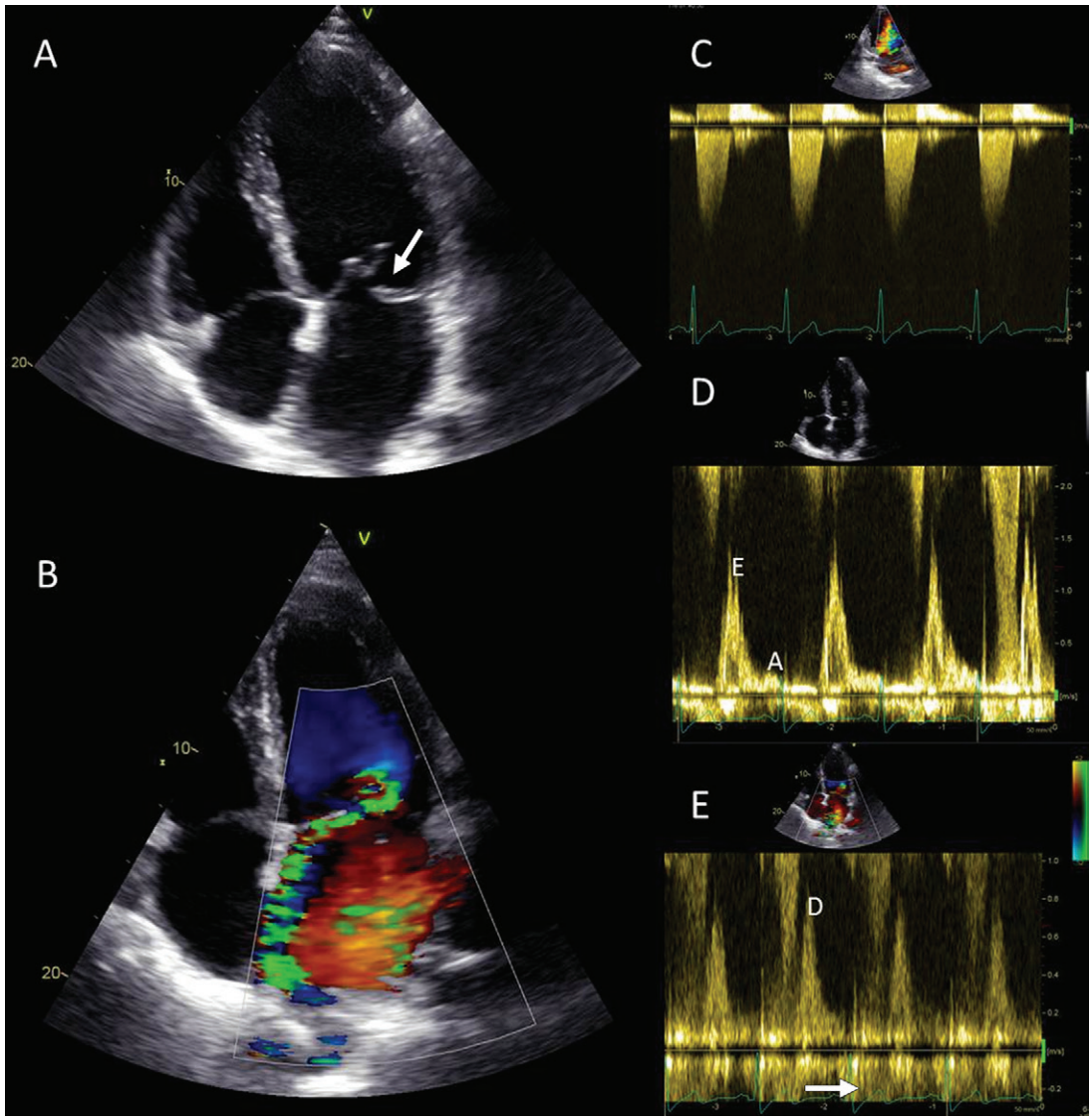

Figure 4: Assessment of mitral regurgitation with echocardiography. *A,* Four-chamber transthoracic echocardiography image in a 63-year-old man with severe mitral regurgitation caused by prolapse of the posterior mitral leaflet (arrow) leading to an eccentric regurgitant jet toward the interatrial septum on, *B,* color flow Doppler scan. On, *C,* continuous wave Doppler, the spectral Doppler signal is dense and triangular and on, *D,* pulsed wave Doppler, note the prominent early diastolic (*E*) wave over the late diastolic (*A*) wave on transmitral flow and, *E,* the systolic flow reversal of the pulmonary vein flow (arrow) followed by the diastolic flow (*D*).

postero-lateral angle greater than 45° (both indicating significant restriction of the posterior mitral leaflet); *(b)* local LV remodeling—interpapillary muscle distance greater than 20 mm, posterior papillary-fibrosa distance greater than 40 mm, and lateral wall motion abnormalities; and *(c)* global LV remodeling—end diastolic diameter greater than 65 mm, end systolic diameter greater than 51 mm, systolic sphericity index greater than 0.7. These parameters can all be measured at echocardiography, CT, and MRI (12,13).

Annular Sizing

CT affords the opportunity for true isometric volumetric 3D imaging of the LV, left atrium, and the mitral valve and subvalvular apparatus. CT is established in the routine work-up for TAVR, with superior clinical outcomes with CT sizing than with echocardiographic annulus sizing (40). Building on prior experience in aortic intervention, CT has been used in all studies to date in assessing patients for TMVR (41–44). Although CT lacks the capacity to provide hemodynamic information for TMVR, it provides highly reproducible evaluation of the 3D geometry of the mitral valve annulus. CT is also sensitive for the detection of annular calcification (45).

CT performed for mitral valve and annulus assessment requires electrocardiogram (ECG) synchronized acquisition (as per Table E1 [online]), coverage limited to the heart, coverage of the entire cardiac cycle with no dose modulation, contrast-enhanced scanning triggered from the LV (rather than the aorta as typically used in TAVR preassessment), a prolonged injection to ensure that there is adequate contrast opacification of the right heart so as to allow assessment of the interatrial septum if a

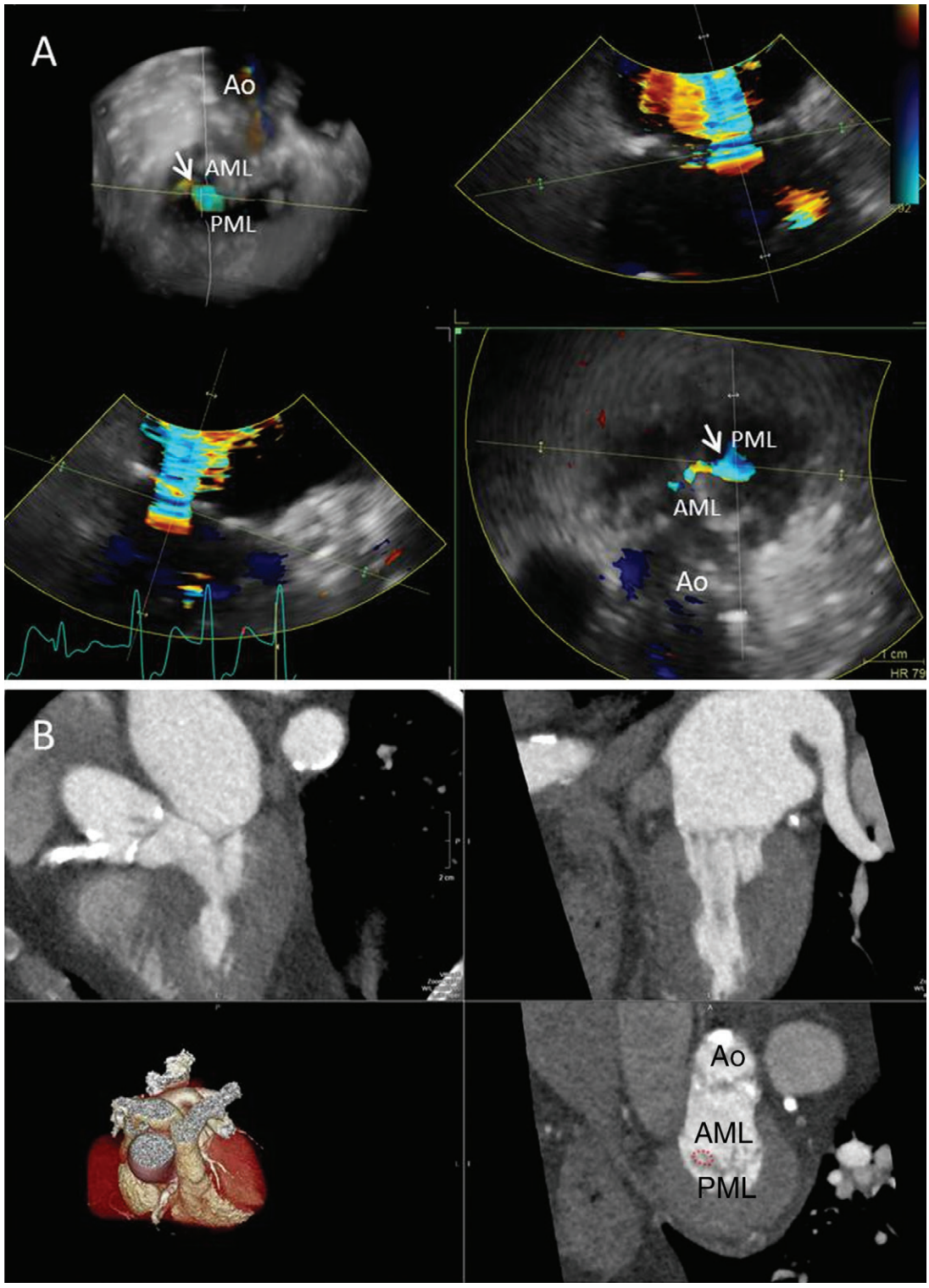

Figure 5: Quantification of mitral regurgitant volume with three-dimensional (3D) imaging techniques in an 87-year-old patient with moderate mitral regurgitation due to lack of medial coaptation (*A3–P3*, arrow in *A*, top left image). *A*, On color Doppler 3D transesophageal echocardiograms, the 3D full-volume data are presented in multiplanar reformation planes oriented across the vena contracta of the regurgitant jet. Arrow = the regurgitant orifice area. *B*, On multidetector row CT scans, the multiplanar reformation planes are aligned across the mitral leaflet coaptation line. Note the orifice area (red dotted circle) located at the same level *(A3–P3)*. AML = anterior mitral leaflet, *Ao* = aortic valve, *PML* = posterior mitral leaflet.

transseptal approach is being considered (typically achieved with a single breath hold following injection of 80–110 mL of intravenous contrast media at 4–5 mL/sec and a biphasic injection [contrast material and saline]) (46). Tube voltage and tube current should be adapted to body habitus as per routine cardiac CT protocols (47). A complimentary nongated low-dose chest

CT can be considered to count rib spaces if ECG-gated acquisition is limited to the heart and a transapical approach is to be used (see section Apex Localization and Septal Puncture).

With CT, assessment of the mitral valve annulus can either be performed by using a true saddle-shaped area and perimeter or by utilizing a standardized exclusion of the anterior horn. Exclusion of the anterior horn allows assessment by using the "D-shaped" concept of the mitral annulus, with truncation of the anterior horn at the level of the fibrous trigones (45). Both can be achieved by stepwise placement of seeding points at regular intervals along the mitral annulus. This creates a 3D model of the mitral annulus from which measurement of the annulus area, perimeter, and septal-lateral and intercommisural distance can be performed. Identification of the trigones then allows truncation of the anterior horn at the level of the fibrous trigones creating the trigone-to-trigone distance (Fig 7). While highly reproducible, such an approach requires specialized software. An alternate approach is a manual technique following a similar technique to that used for obtaining the aortic valve annular plane. This involves sequential identification of the two fibrous trigones followed by the free edge annular ring insertion point (Fig 8) (47).

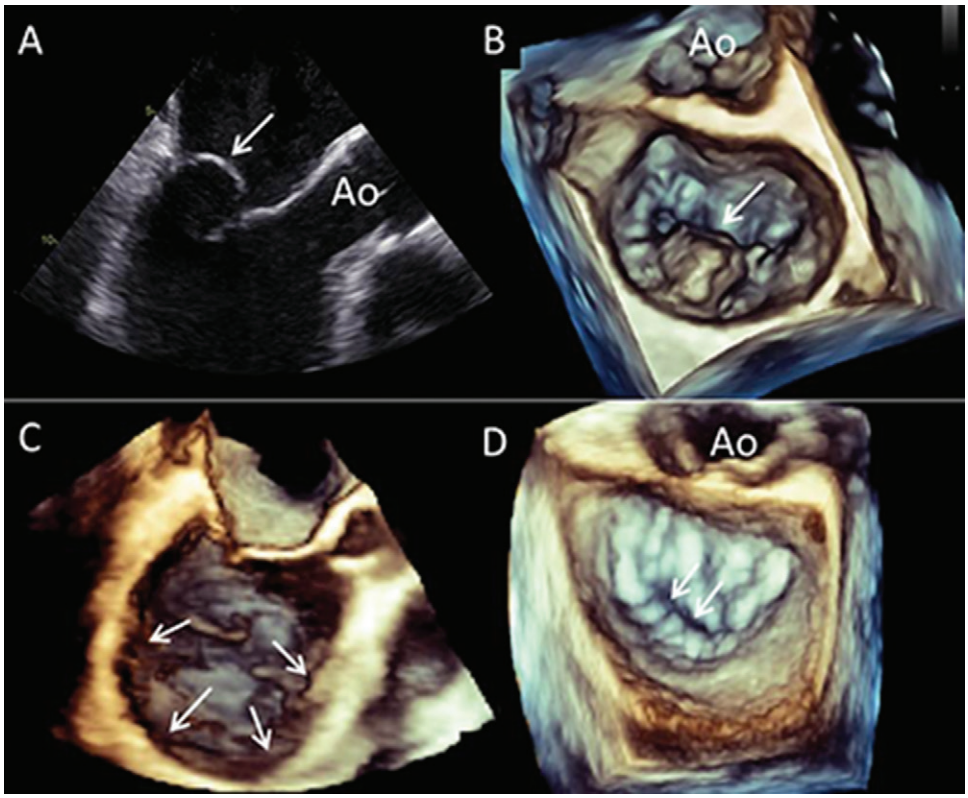

Figure 6: Mitral regurgitation mechanism. *A,* Two-dimensional transesophageal echocardiography; example of primary mitral regurgitation caused by prolapse of the posterior mitral leaflet (arrow). *B,* On three-dimensional transesophageal echocardiogram, the en face view of the mitral valve permits exact location and extent of the prolapsing scallop (central scallop P2, arrow). *C,* Example of secondary mitral regurgitation caused by dilatation of the left ventricle (arrows) and subsequent tethering of the leaflets. *D,* The en face view of the mitral valve on three-dimensional transesophageal echocardiogram shows lack of coaptation between the anterior and posterior leaflets and the central level (arrows). *Ao* = aortic valve.

A number of parameters are integrated into annular sizing reports and help inform device selection. These include the projected two-dimensional area, perimeter, intercommissural, septal-lateral, and intertrigonal distances. The relevance of each of these annular measurements varies across device platforms. The Tiara device (Neovasc) with its D-shaped configuration is highly reliant on the intercommissural distance, as well as the projected annular perimeter. The CardiAQ-Edwards TMV (Edwards Lifesciences) is sized based on the largest annular diameter (16). Given the early stage in the maturation process of TMVR, ongoing investigation is needed to better define the sizing requirements needed for these various devices as was the case for TAVR devices.

While CT currently holds hegemony in annular assessment prior to the procedure, 3D transesophageal echocardiography (TEE) sizing of the mitral annulus in the context of TMVR has shown good intraobserver and interobserver reproducibility and correlation with CT. Mak and colleagues performed an analysis of 41 subjects with mitral regurgitation who were being evaluated for transcatheter interventions and showed strong correlation (r = 0.69 and r = 0.71; $P <$ .0001) and no systematic bias (0.77 mm ± 3.8 [95% confidence interval: −6.7 mm, 8.2 mm] and −1.5 mm ± 3.1 [95% confidence interval: −4.6 mm; 7.6 mm]) between annular measurements obtained by using 3D TEE and those obtained by using CT (48). Given the high temporal resolution of TEE, it can provide important insight into mitral annular dynamism and function. Normal dynamics of the mitral annulus are characterized by early systolic contraction and more pronounced saddle shape, both of which contribute to leaflet coaptation. In primary mitral regurgitation due to myxomatous valve disease, early contraction is reduced, the intercommisural diameter increases, and the saddle shape becomes flatter leading to mitral incompetence. In secondary mitral regurgitation, the mitral annulus is significantly less dynamic (49,50). The presence of mitral annulus calcification also leads to loss of annular contraction and loss of early systolic folding along the intercommissural diameter (Fig 9) (51).

Landing Zone Characterization

CT plays an important role in defining the landing zone for TMV procedures. CT can provide detailed and clear definition of the extent and severity of annular calcium, which can help determine device suitability (Fig 9). Exuberant mitral

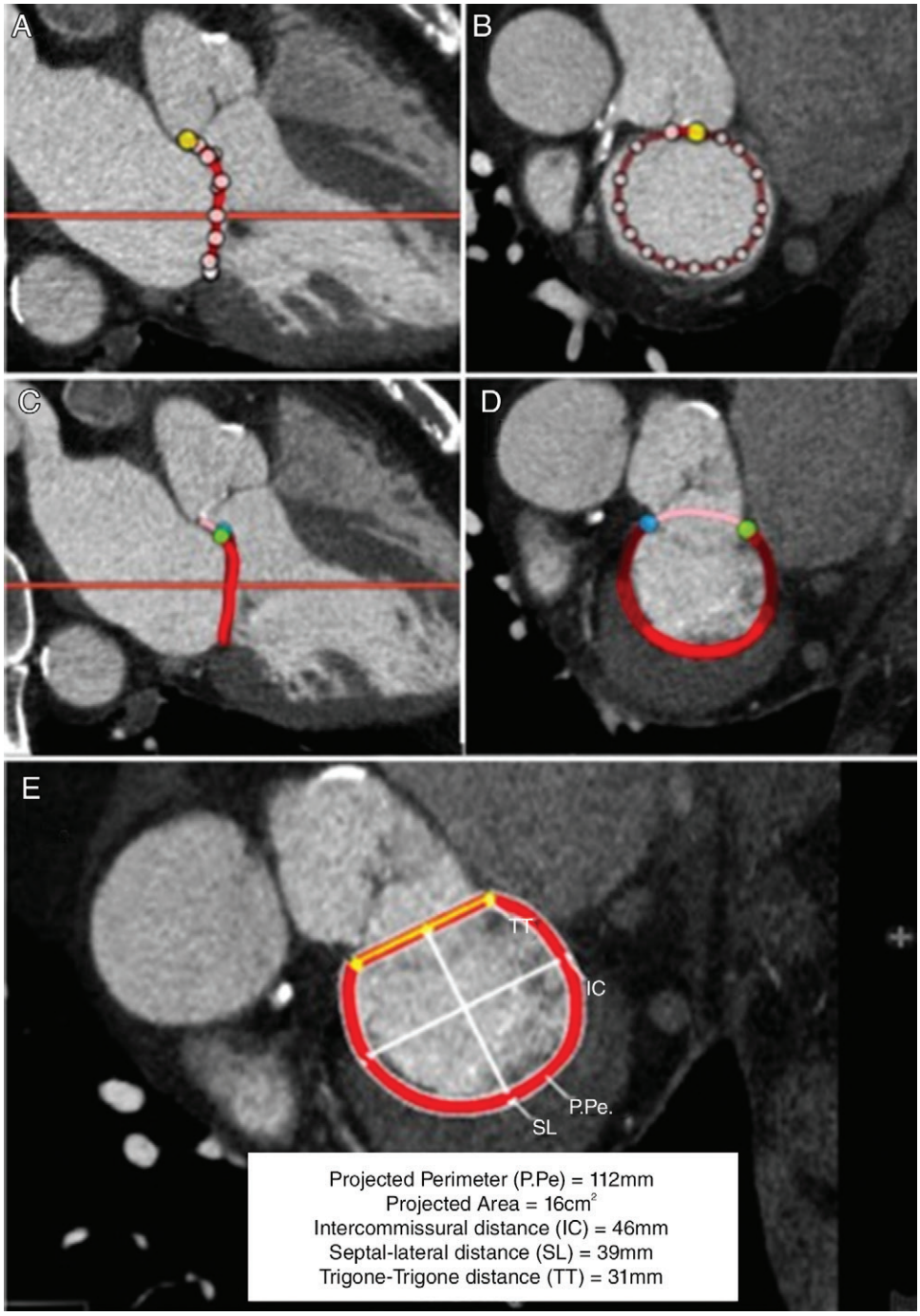

Figure 7: D-shaped mitral annular segmentation and measurements. Three-dimensional segmentation is performed by manually placing seeding points along the annulus as it is rotated in 22° increments around the, *A,* long-axis plane and by cross-referencing with the corresponding, *B,* short-axis images. The resultant saddle-shaped mitral annulus contour is composed of the anterior (pink contour) and posterior (red contour) horns demarcated by the fibrous trigones (green = medial; blue = lateral, filled circles) as shown in *C* and *D*. For transcatheter mitral valve planning, the D-shaped annulus, formed by truncation of the anterior horn, is used to determine the two-dimensionally projected annular perimeter and area, as well as intercommissural *(IC)*, septal-lateral *(SL)*, and trigone-trigone *(TT)* distances as shown in *E*.

annular calcification (MAC) poses an issue for CT regarding segmentation of the annulus. In the case of MAC, correct definition of the boundary of the blood pool and calcified annular segments can be very difficult. However, MAC also poses issues for transesophageal echocardiography because tissue characterization is a known weakness of echocardiography (5,51). The significance of MAC varies by the intended approach of intervention. Extensive MAC involving at least 75% of the circumference of all four quadrants of the annulus is a prerequisite for the implantation of aortic transcatheter

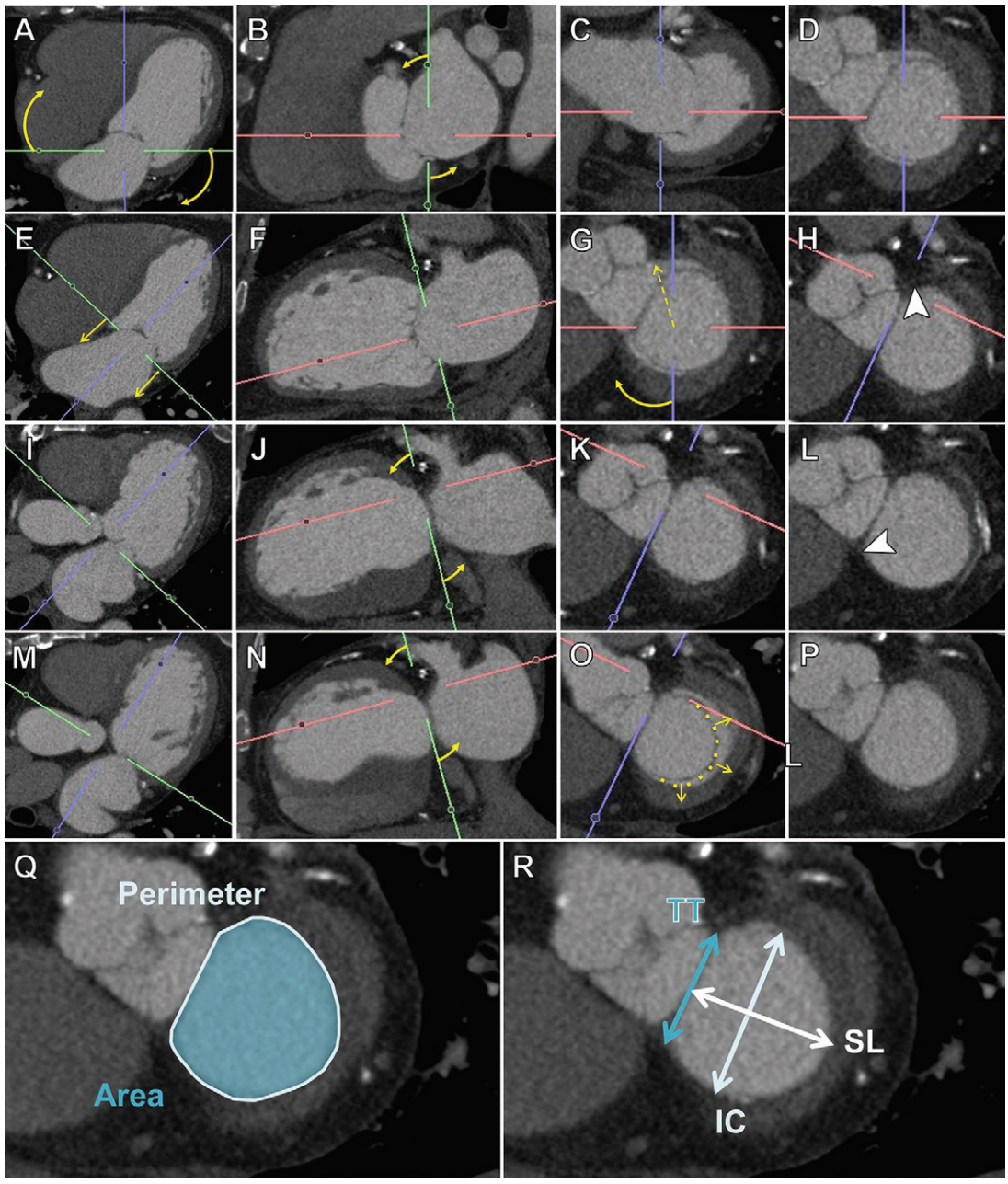

Figure 8: Manual technique for obtaining a planar view through the mitral annulus from which the annular area, trigone-trigone, and septal-lateral distances can be obtained. After approximately centering the cursor over the mitral valve *(A–C)*, an approximate mitral planar view is obtained by aligning the image to the atrioventricular groove *(E–G)*. The left fibrous trigone is identified by panning the short-axis oblique view through the upper ventricle *(E–G)* until the well-defined triangle of the trigone comes into view (*H*, arrowhead). The image should then be centered on the left trigone and the vertical axis rotated so that it aligns with the approximate location of the right trigone *(G)*. The right fibrous trigone is then obtained by rotating the vertical axis *(I–K)* until the second well-defined triangular trigone comes into view (*L*, arrowhead). Finally, the free edge of the annulus (dashed yellow line) is obtained by rotating the horizontal axis *(M–O)* until its insertion in the ventricle *(P)*. From this segmentation, the annular area and perimeter *(Q)* and trigone-trigone, septal-lateral, and intercommisural distances can be measured *(R)*. Curved arrows indicate rotating the image and straight arrows indicate moving the plane without altering its angulation. The right-hand images *(D, H, L, P)* are the approximate appearance the annulus should assume at each step of the process. *TT* = trigone-trigone, *SI* = septal-lateral, and *IC* = intercommisural.

heart valves to treat mitral stenosis to provide sufficient purchase for these devices as they anchor themselves based on radial force and friction (Fig 10) (52). Conversely, severe MAC has been a contraindication in studies to date examining the clinical feasibility of TMVR valves currently in production. Importantly, MAC is a heterogeneous process, with calcium varying not only in distribution but in density. Some calcifications are extremely dense and rock-like, while a caseous

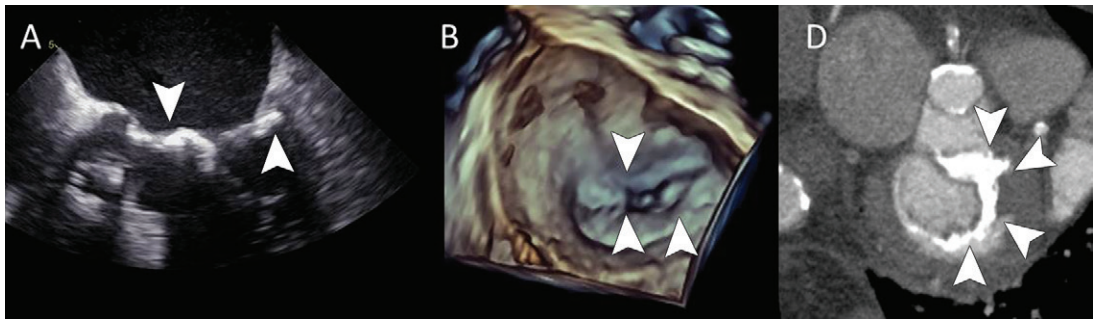

Figure 9: Mitral annulus calcification. *A,* On two-dimensional echocardiogram, calcifications of the mitral annulus, extending to the anterior mitral leaflet, are shown (arrowheads). *B,* On three-dimensional echocardiogram, the software provides different color shades to indicate thickness of the mitral valve most probably caused by calcification. In this example, the calcifications affect the most lateral levels of the anterior and posterior mitral annulus (arrowheads). *C,* On multidetector row CT scan, the calcifications are clearly visualized on the same locations as on echocardiogram involving both the annulus but extending to the left fibrous trigone, anterior mitral leaflet, and, to a lesser degree, the posterior leaflet (arrowheads).

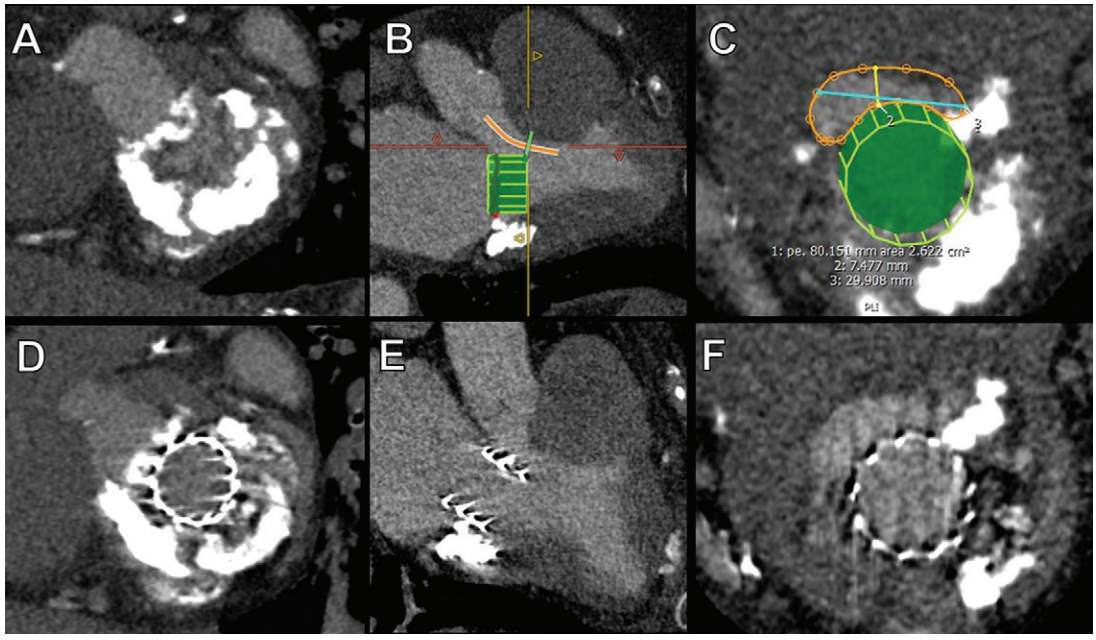

Figure 10: Valve in mitral annular calcification work-up. *A,* Severe mitral annulus calcification involving more than 75% of the annulus circumference, thereby providing enough coverage to provide anchorage for insertion of an aortic transcatheter heart valve. *B* and *C,* Images demonstrate a satisfactory neo-left ventricular outflow tract (LVOT) following the insertion of a simulated 26-mm valve. *D–F,* Postprocedural CT scans show close agreement with the preprocedural simulation, although the neo-LVOT is even more spacious due to an unanticipated inferolateral canter to the inserted valve.

pattern is also quite common. The impact on device counter bearing is very much dependent on the type and density of MAC. Unfortunately, the present classification of MAC is qualitative, and there is little evidence to allow estimation of the potential impact this may have on device deployment, positioning, and expansion.

Currently an evidence-based approach on how to handle this calcification, whether to partially include irregularities and/or nodules in the annular area or to exclude it entirely is not available. Given this limitation both in CT and transesophageal echocardiography, it may be more appropriate to focus on defining a clear process for mitral annular segmentation that is highly reproducible rather than focusing on what is anatomically correct. Clearly defined methodology to ensure consistent and reproducible segmentation of MAC will afford the opportunity to correlate these measurements with downstream procedural outcomes and generate the data necessary to provide more robust guidance in this challenging area. If segmentation remains nonstandardized, then it will be impossible to understand how underlying anatomy impacts device expansion, sealing, and eventually clinical outcomes. As such, the authors advocate that the annulus is defined as a harmonious, smoothly marginated structure. In essence, this approach ignores protruding

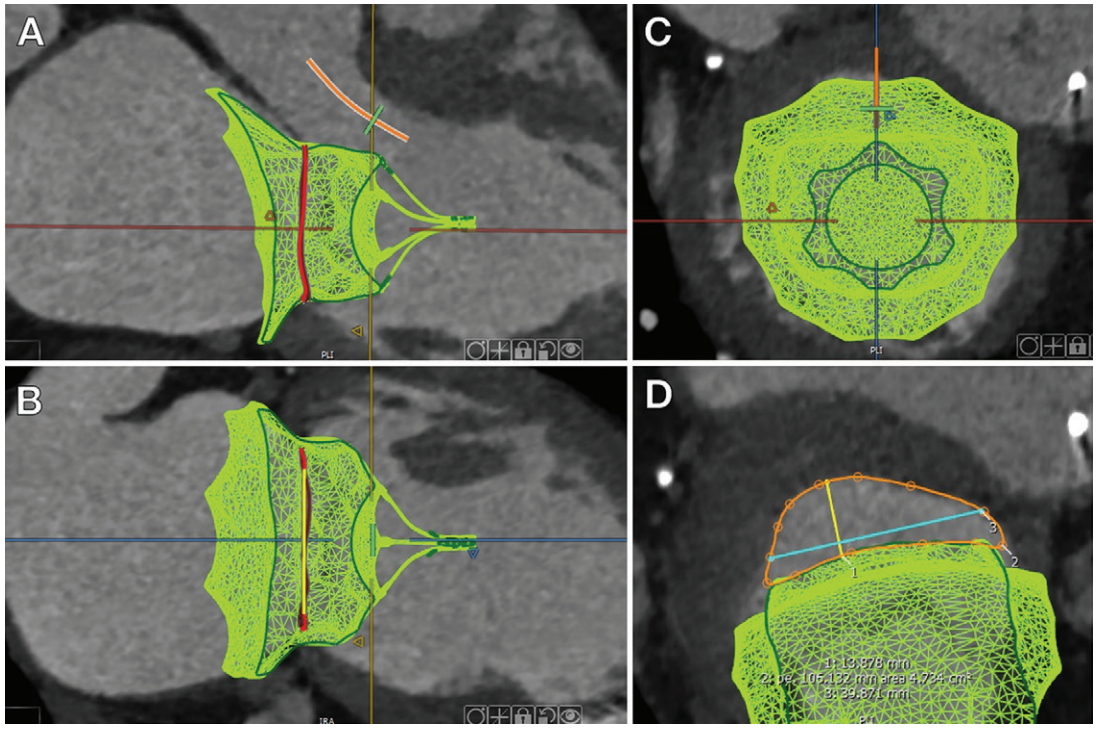

Figure 11: Prediction of risk of left ventricular obstruction following mitral valve insertion. *A,* Three-chamber, *B,* two-chamber, and, *C,* en face views of the mitral annulus (red line) with a three-dimensional simulation of the intended device to be inserted (green meshwork) seated within the annulus at end systole. A centerline is prescribed through the neo-left ventricular outflow tract (orange line in *A*), and, *D,* at the point where the simulated valve comes closest to the septal wall, the area is measured (orange line).

nodules of calcification during segmentation, thus avoiding an individualized and nonstandardized segmentation approach to such variant anatomy (Fig 10).

CT also plays an important role in defining other landing zone features that are relevant to determine the likelihood of device capture and sealing. CT can depict and accurately size the posterior shelf that commonly develops in the setting of functional mitral regurgitation, particularly in the setting of prior infarction (46,48). This posterior shelf is needed to assist with the capture of some of the self-expanding devices relying on a persisting posterior shelf throughout the cardiac cycle (10,46). Features like mitral annular disjunction (whereby the mitral annulus becomes separated from the atrioventricular junction) and mitral valve tenting, traditionally evaluated with echocardiography, can also be identified and characterized with increasing accuracy and detail.

LVOT Obstruction Assessment

LVOT obstruction during transcatheter mitral intervention in the treatment of native mitral valves, valve in ring, and valve in valve is a feared and potentially catastrophic complication (52,53). The mechanisms of obstruction are broad and complex and only modestly understood. Patient-specific variables such as ventricular size, septal thickness, anterior mitral valve leaflet length, change in ejection fraction, and volume status all play a role as do structural and design characteristics of the implanted device. Procedural factors such as device canting or tilting toward the LVOT and inability to deploy the valve in a coaxial fashion will also greatly impact the postimplant LVOT space. In addition, LVOT obstruction can be dynamic, mainly due to systolic anterior motion of the anterior mitral valve leaflet. Importantly, anatomic assessment with CT, including simulation of device implantation, is unable to confidently predict what will happen with the anterior mitral valve leaflet following TMVR (54,55).

CT can help discriminate the risk of postimplant LVOT obstruction. The LVOT remodels following valve deployment by undergoing elongation, with the anatomy defined by the deployed valve/leaflet and the ventricular septum. Given the anatomic remodeling of the LVOT, it seems more appropriate to provide a new designation for this anatomic compartment; we refer to this space as the neo-LVOT. This neo-LVOT is defined by drawing a center line through the middle of the residual space between the septum and simulated implanted transcatheter device. The evaluation should then evaluate the residual space defined in a perpendicular fashion to the centerline of the LVOT. The neo-LVOT is then determined at the site of the greatest encroachment and narrowing. The lower bound of neo-LVOT narrowing that will allow for acceptable postimplant gradients is not well established. As such, the field has relied on evidence from hypertrophic cardiomyopathy based on which a conservative threshold of 1.5 cm^2 has been adopted for consideration of being at risk for postprocedural LVOT obstruction (56). In the early experience with TMVR, end systolic imaging has been favored for the evaluation of the neo-LVOT as it yields the most conservative data (57) and thus allows for thoughtful discussion

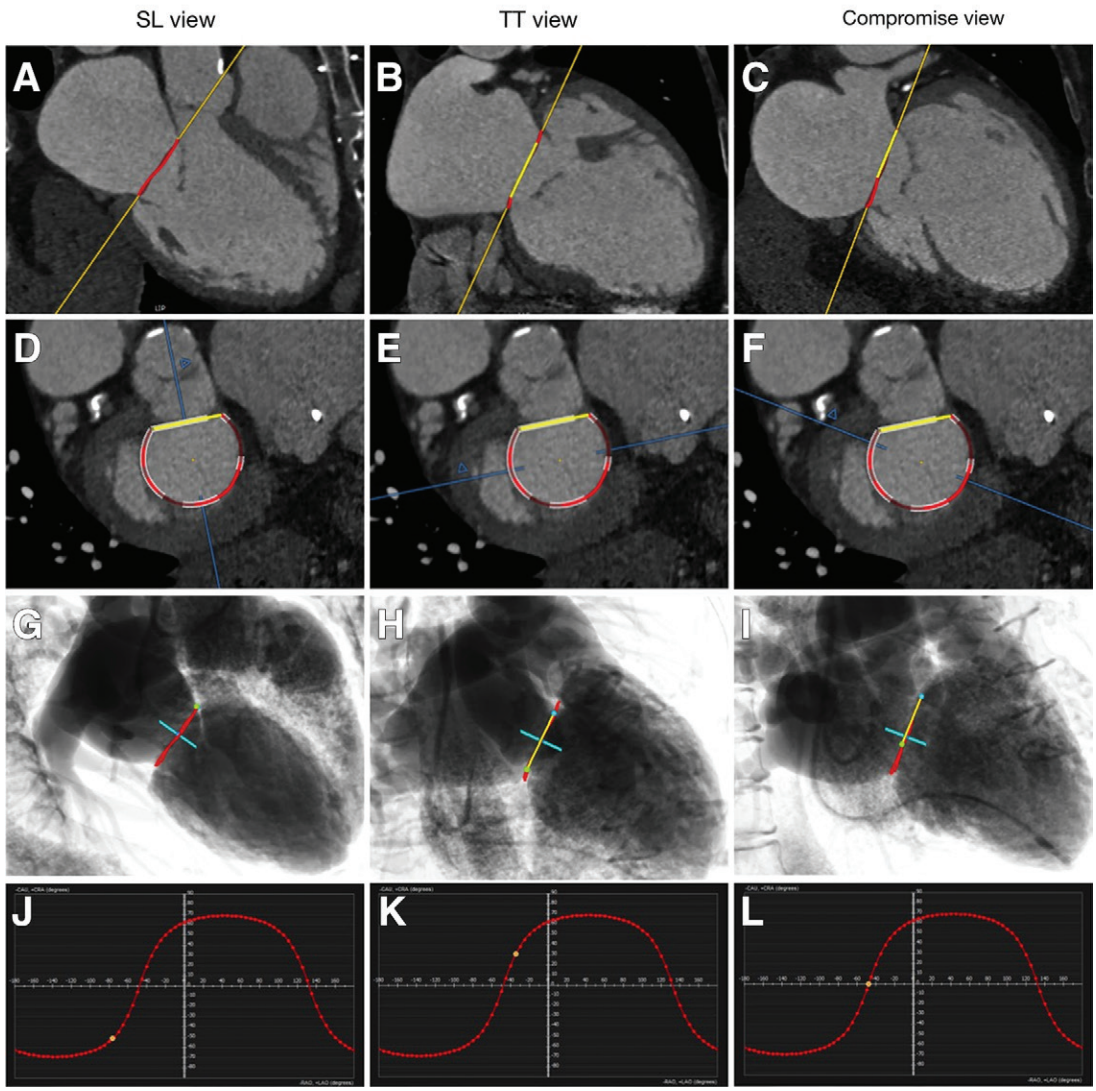

Figure 12: Prediction of fluoroscopic angulation for coplanar deployment. *A–C,* Long-axis views of the mitral valve obtained aligned to the septal-lateral line *(SL)*, trigone-to-trigone line *(TT)*, and the commonly used compromise view. *D–E,* Annular views, with the blue line demonstrating how A–C views intersect the annulus. *G–I,* Images show how these views would appear on invasive angiograms based on three-dimensional CT data. *J–K,* Images demonstrate the sinusoidal path the c-arm would follow as it rotates around the patient to always provide a tangential valvular view, with the x-axis describing the LAO-RAO tilt required and the y-axis describing the CRA-CAU tilt required. The yellow dots demonstrate where each of the A–C views lie on this axis. *LAO* = left anterior oblique, *RAO* = right anterior oblique, *CRA* = cranial, *CAU* = caudal.

prior to valve insertion, which seems prudent in the early stages of clinical adoption of this technology. Unfortunately, there are little outcome data available validating this threshold currently, owing to limited clinical experience and exclusion of patients with narrow predicted neo-LVOT.

The image analysis for the prediction of the neo-LVOT obstruction is similar across the treatment of the various disease states, be it transcatheter valve in valve, valve in ring, MAC, or TMVR. The landing zone needs to be defined, and the size and type of the implanted device should be determined. There are subtle differences, though, in the mechanism and site of neo-LVOT obstruction in these different procedures. When inserting an aortic transcatheter heart valve within a failed bioprosthetic valve, the new transcatheter valve results in the displacement of the surgical valve leaflets to oppose the surgical stent struts, resulting in a covered stent in the LVOT. Given this, a simulation of a more atrial deployment of the transcatheter heart valve will have no impact on the degree of LVOT encroachment. In valve in ring and valve in MAC, the mechanism of neo-LVOT encroachment relates to displacement of the anterior leaflet of the mitral valve, and thus atrial offset of the transcatheter valve can help mitigate the risk of LVOT obstruction; therefore simulating the intended transcatheter heart valve to mimic the intended degree of atrial offset is important. When evaluating neo-LVOT obstruction risk in TMVR, it is important that the intended device be simulated. A conical structure is adequate when a traditional aortic transcatheter heart valve is being used in valve-in-valve and valve-in-MAC

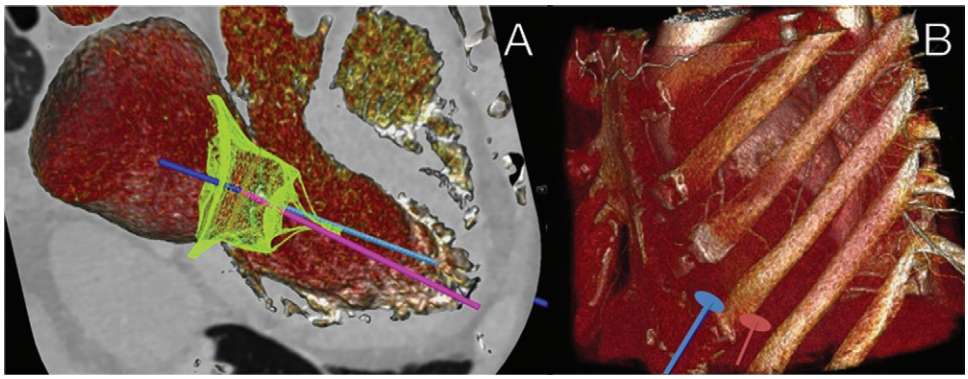

Figure 13: Prediction of optimal point of access for an en face mitral annular approach. *A,* A true transapical approach (blue line) would result in a 17° off center angulation with respect to the mitral annulus. *B,* The red line, representing a tangential projection from the centroid of the mitral annular plane, would enable a true direct approach and requires access to be achieved one rib space superior to the left ventricle apex.

procedures. However, with TMVR, the best results will be obtained by using dedicated software plug-ins that allow virtual generation of the shape and size of the actual valve to be used (Fig 11). Such an approach allows for a patient- and device-specific neo-LVOT to be calculated, and thus a more accurate assessment of the risk of obstruction of the neo-LVOT.

Predicting Fluoroscopic Angulations

During any transcatheter cardiac intervention it is important for the proceduralist to deploy his or her device using fluoroscopic angulation that lies perpendicular to the mitral annulus, as obliquity can lead to an inaccurate appreciation of the true valve plane, and therefore, insertion of the device too far into the atrium or ventricle. For TMVR, this requires accurate imaging of the mitral annular plane and the alignment of the septal-lateral and intercommissural lines to ensure coaxial deployment. Similar to TAVR and left atrial appendage occlusion, CT has been shown to be helpful in generating patient-specific coplanar curves, allowing for coaxial deployment of the TMVR device (58–60) (Fig 12). In addition, by using centerline mapping, relevant adjacent anatomy such as the location of the coronary sinus and left circumflex coronary artery can be defined and transmitted to the hybrid, or to provide a roadmap during the procedure and define patient-specific risk.

Apex Localization and Septal Puncture

At present, the majority of devices under evaluation in feasibility studies have used transapical access (16). To help prevent device canting and resultant LVOT obstruction, inadequate sealing, and paravalvular regurgitation, the access point chosen should allow for a perpendicular delivery of the transcatheter mitral device to the mitral annulus. CT may play an important role in helping identify the appropriate access point in advance of the procedure. Early experiences have highlighted that there is significant variability regarding the appropriate access point across subjects and mechanisms of mitral regurgitation. Blanke and colleagues evaluated 54 subjects who were being evaluated for TMVR and noted that the mean distance between the "orthogonal" MV access point and the true apex was 17.6 mm ± 7.7 (range, 1.9–38.9 mm) for the entire cohort and 18.0 mm ± 7.9 and 16.9 mm ± 7.5 for patients with mitral regurgitation and degenerative mitral valve disease, respectively. The orthogonal LV access points offset in an anterolateral (n = 22, 40.7%) and anterior (n = 16, 29.6%) location, with the appropriate orthogonal LV access point showing significant interindividual variability and most commonly does not align with the true LV apex (61). By projecting an orthogonal line from the centroid of the mitral annulus and a mitral-apical line, the point of access that would allow a true en face approach to the mitral annulus can be generated either in relation to the true LV apex or in relation to adjacent landmarks such as the ribs and distance from the midline (Fig 13).

Additional Information

Further valve-specific measurements depend largely on the device being implanted. The reporting cardiac imager should be aware of the devices being considered for implantation at their local institute. Examples of such variations include the need to report the relationship of the left circumflex artery to the annulus in those being assessed for Cardioband insertion to minimize risk of coronary injury or the presence of posterior leaflet length and presence of leaflet tip calcification in those being considered for MitraClip (22,62).

In addition to valvular assessment, assessment of LV dimensions and function, left atrial volume, and pulmonary artery pressures is of importance in the clinical decision making in patients with severe mitral regurgitation. In severe primary mitral regurgitation, the presence of LV ejection fraction of 60% or greater is an indication for surgery. In asymptomatic patients, the presence of an LV end systolic diameter of 40 mm or greater, left atrial dilatation (≥ 60 mL/m^2), and increased systolic pulmonary pressures (> 50 mmHg at rest or ≥ 60 mmHg during exercise) may be considered to indicate surgery when there is a high likelihood of durable valve repair (7). These variables can be assessed accurately and reproducibly with echocardiography (63). Similarly, right ventricular function has been shown to be prognostically important in patients with severe mitral regurgitation (64). Finally, in transcatheter mitral repair the mitral

Table 2: Report Framework for Preprocedural CT

Anatomic Structure and Metric	Detail
Annulus	
Qualitative	Mitral annular calcification
	Extent of coverage according to segmental distribution (A1–A3 and P1–P3)
	Mitroannular disjunction
Quantitative*	Area (+)
	Perimeter (+)
	Intercommisural distance (+)
	Septal-lateral distance (+)
	Trigone-trigone distance (-)
	Fluoroscopic angulation (+)
	Intercommisural view, compromise view, en face view
Leaflets	
Qualitative	Leaflet thickness
	Prolapse/flail segments
	Individually for A1–3 and P1–3
	Leaflet tethering
	Leaflet calcification
	Location (tip versus hinge)
	Extent
Quantitative*	Leaflet length (-)
	Coaptation distance (-)
	Tenting height/area (-)
Subvalvular apparatus	
Qualitative	Number and insertion points
	Presence of bifid muscles or direct muscular insertions
Quantitative*	Interpapillary distance (-)
	Chordae length (-)
Left ventricle	
Qualitative	Global function
	Regional wall motion abnormalities
	Myocardial scarring/calcification
Quantitative*	
	Left ventricular end diastolic and end systolic internal diameter (+)
	The latter should be reported at the distal most aspect of the anticipated valve to be inserted
	Long-axis length (-)
	Neo-LVOT area (+)
	Aortomitral angle (-)
	Ejection fraction (-)
	Apical location in relation to midline and intercostal space (-)
Cardiac	
Qualitative	Incidental findings
	Left atrial appendage thrombus, interatrial septal aneurysm, ASD/PFO, relationship of the left circumflex artery to coronary sinus
Quantitative*	Left atrial dimensions (-)
	Right ventricular ejection fraction (-)
Extracardiac	
Qualitative	Incidental findings
Quantitative*	Venous dimensions
	Venous stenosis is exceptionally rare in the absence of prior thombosis or prolonged/repeated instrumentation and diameters are highly variable dependent on respiratory status thus should not be routinely performed (-)

* Quantitative metrics are marked as essential (+) when they are common to the majority of transcatheter mitral valve interventions and minor (-) when they are specific to select devices or for prognostic purposes rather than required for device selection.

valve is accessed through transseptal puncture, and while most current TMVRs are inserted via a transapical approach, significant advances are being made in transseptal approaches. Thus evaluation of the anatomy of the interatrial septum will become of increasing importance. The analysis of this is useful to anticipate the site of the puncture and minimize complications such as puncture of the aorta (65). An aneurysmal septum, a patent foramen ovale or atrial septal defects may pose challenges for TMV procedures (66). A suggested reporting checklist for preprocedural CT is provided in Table 2.

Conclusion

Rapid advancements in TMV procedures have driven an increasing demand for noninvasive imaging to help assist in evaluation and procedural planning. Echocardiography remains the imaging test of choice for the diagnosis of mitral valvular disease and the gradation of its severity. However, there is growing use of multidetector CT as a tool that can provide incremental information for annular sizing, landing zone characterization, risk stratification for LVOT obstruction, access point localization, and fluoroscopic angles to guide the procedure.

Disclosures of Conflicts of Interest: **J.R.W.M.** disclosed no relevant relationships. **P.B.** Activities related to the present article: disclosed no relevant relationships. Activities not related to the present article: consultancy fees from Edwards Lifesciences, Tendyne, and Circle Cardiovascular Imaging and received payment from Edwards Lifesciences for lectures including service on speakers bureaus and for development of educational presentations. Other relationships: disclosed no relevant relationships. **C.N.** disclosed no relevant relationships. **V.D.** Activities related to the present article: disclosed no relevant relationships. Activities not related to the present article: institution received grants/pending grants from Medtronic, Biotronic, Boston Scientific, and Edwards Lifesciences; author received payment for lectures including service on speakers bureaus from Abbott Vascular. Other relationships: disclosed no relevant relationships. **J.J.B.** Activities related to the present article: disclosed no relevant relationships. Activities not related to the present article: institution received grants/pending grants from Medtronic, Biotronic, Boston Scientific, and Edwards Lifesciences. Other relationships: disclosed no relevant relationships. **J.L.** Activities related to the present article: institution received a grant from Edwards Lifesciences, Medtronic, Abbott, and Neovasc; author received consulting fee or honorarium and support for travel to meetings for the study or other purposes from Edwards Lifesciences. Activities not related to the present article: consultancy fees and stock/stock options from Circle Cardiovascular Imaging and Heartflow. Other relationships: disclosed no relevant relationships.

References

1. Nkomo VT, Gardin JM, Skelton TN, Gottdiener JS, Scott CG, Enriquez-Sarano M. Burden of valvular heart diseases: a population-based study. Lancet 2006;368(9540):1005–1011.
2. Nishimura RA, Vahanian A, Eleid MF, Mack MJ. Mitral valve disease: current management and future challenges. Lancet 2016;387(10025):1324–1334.
3. Rossi A, Dini FL, Faggiano P, et al. Independent prognostic value of functional mitral regurgitation in patients with heart failure: a quantitative analysis of 1256 patients with ischaemic and non-ischaemic dilated cardiomyopathy. Heart 2011;97(20):1675–1680.
4. Ling LH, Enriquez-Sarano M, Seward JB, et al. Clinical outcome of mitral regurgitation due to flail leaflet. N Engl J Med 1996;335(19):1417–1423.
5. Abramowitz Y, Jilaihawi H, Chakravarty T, Mack MJ, Makkar RR. Mitral annulus calcification. J Am Coll Cardiol 2015;66(17):1934–1941.
6. Ho SY. Anatomy of the mitral valve. Heart 2002;88(Suppl 4):iv5–iv10.
7. Nishimura RA, Otto CM, Bonow RO, et al. 2017 AHA/ACC focused update of the 2014 AHA/ACC guideline for the management of patients with valvular heart disease: a report of the American College of Cardiology/American Heart Association Task Force on Clinical Practice Guidelines. Circulation 2017;135(25):e1159–e1195.
8. Zoghbi WA, Adams D, Bonow RO, et al. Recommendations for noninvasive evaluation of native valvular regurgitation: a report from the American Society of Echocardiography developed in collaboration with the Society for Cardiovascular Magnetic Resonance. J Am Soc Echocardiogr 2017;30(4):303–371.
9. Thavendiranathan P, Phelan D, Thomas JD, Flamm SD, Marwick TH. Quantitative assessment of mitral regurgitation: validation of new methods. J Am Coll Cardiol 2012;60(16):1470–1483.
10. Cavalcante JL, Rodriguez LL, Kapadia S, Tuzcu EM, Stewart WJ. Role of echocardiography in percutaneous mitral valve interventions. JACC Cardiovasc Imaging 2012;5(7):733–746.
11. Naoum C, Blanke P, Cavalcante JL, Leipsic J. Cardiac computed tomography and magnetic resonance imaging in the evaluation of mitral and tricuspid valve disease: implications for transcatheter interventions. Circ Cardiovasc Imaging 2017;10(3):e005331.
12. Delgado V, Tops LF, Schuijf JD, et al. Assessment of mitral valve anatomy and geometry with multislice computed tomography. JACC Cardiovasc Imaging 2009;2(5):556–565.
13. van Rosendael PJ, Katsanos S, Kamperidis V, et al. New insights on Carpentier I mitral regurgitation from multidetector row computed tomography. Am J Cardiol 2014;114(5):763–768.
14. Blanke P, Naoum C, Webb J, et al. Multimodality imaging in the context of transcatheter mitral valve replacement: establishing consensus among modalities and disciplines. JACC Cardiovasc Imaging 2015;8(10):1191–1208.
15. Garbi M, Monaghan MJ. Quantitative mitral valve anatomy and pathology. Echo Res Pract 2015;2(3):R63–R72.
16. Regueiro A, Granada JF, Dagenais F, Rodés-Cabau J. Transcatheter mitral valve replacement: insights from early clinical experience and future challenges. J Am Coll Cardiol 2017;69(17):2175–2192.
17. Rodriguez F, Langer F, Harrington KB, et al. Importance of mitral valve second-order chordae for left ventricular geometry, wall thickening mechanics, and global systolic function. Circulation 2004;110(11 Suppl 1):II115–II122.
18. Baumgartner H, Falk V, Bax JJ, et al. 2017 ESC/EACTS guidelines for the management of valvular heart disease. Eur Heart J 2017;38(36):2739–2791.
19. Goldstein D, Moskowitz AJ, Gelijns AC, et al. Two-year outcomes of surgical treatment of severe ischemic mitral regurgitation. N Engl J Med 2016;374(4):344–353.
20. Puls M, Lubos E, Boekstegers P, et al. One-year outcomes and predictors of mortality after MitraClip therapy in contemporary clinical practice: results from the German transcatheter mitral valve interventions registry. Eur Heart J 2016;37(8):703–712.
21. Praz F, Spargias K, Chrissoheris M, et al. Compassionate use of the PASCAL transcatheter mitral valve repair system for patients with severe mitral regurgitation: a multicentre, prospective, observational, first-in-man study. Lancet 2017;390(10096):773–780.
22. Nickenig G, Hammerstingl C, Schueler R, et al. Transcatheter mitral annuloplasty in chronic functional mitral regurgitation: 6-month results with the cardioband percutaneous mitral repair system. JACC Cardiovasc Interv 2016;9(19):2039–2047.
23. Siminiak T, Wu JC, Haude M, et al. Treatment of functional mitral regurgitation by percutaneous annuloplasty: results of the TITAN Trial. Eur J Heart Fail 2012;14(8):931–938.
24. Feldman T, Kar S, Elmariah S, et al. Randomized comparison of percutaneous repair and surgery for mitral regurgitation: 5-year results of EVEREST II. J Am Coll Cardiol 2015;66(25):2844–2854.
25. Nickenig G, Estevez-Loureiro R, Franzen O, et al. Percutaneous mitral valve edge-to-edge repair: in-hospital results and 1-year follow-up of 628 patients of the 2011-2012 Pilot European Sentinel Registry. J Am Coll Cardiol 2014;64(9):875–884.
26. Feldman T, Kar S, Rinaldi M, et al. Percutaneous mitral repair with the MitraClip system: safety and midterm durability in the initial EVEREST (Endovascular Valve Edge-to-Edge REpair Study) cohort. J Am Coll Cardiol 2009;54(8):686–694.
27. Coffey S, Cairns BJ, Iung B. The modern epidemiology of heart valve disease. Heart 2016;102(1):75–85.
28. Thavendiranathan P, Phelan D, Collier P, Thomas JD, Flamm SD, Marwick TH. Quantitative assessment of mitral regurgitation: how best to do it. JACC Cardiovasc Imaging 2012;5(11):1161–1175.
29. Heo R, Son JW, Ó Hartaigh B, et al. Clinical implications of three-dimensional real-time color Doppler transthoracic echocardiography in quantifying mitral regurgitation: a comparison with conventional two-dimensional methods. J Am Soc Echocardiogr 2017;30(4):393–403.e7.
30. Choi J, Heo R, Hong GR, et al. Differential effect of 3-dimensional color Doppler echocardiography for the quantification of mitral regurgitation according to the severity and characteristics. Circ Cardiovasc Imaging 2014;7(3):535–544.
31. Marsan NA, Westenberg JJ, Ypenburg C, et al. Quantification of functional mitral regurgitation by real-time 3D echocardiography: comparison with 3D velocity-encoded cardiac magnetic resonance. JACC Cardiovasc Imaging 2009;2(11):1245–1252.

32. Shanks M, Siebelink HM, Delgado V, et al. Quantitative assessment of mitral regurgitation: comparison between three-dimensional transesophageal echocardiography and magnetic resonance imaging. Circ Cardiovasc Imaging 2010;3(6):694–700.
33. Uretsky S, Gillam L, Lang R, et al. Discordance between echocardiography and MRI in the assessment of mitral regurgitation severity: a prospective multicenter trial. J Am Coll Cardiol 2015;65(11):1078–1088.
34. Mehta NK, Kim J, Siden JY, et al. Utility of cardiac magnetic resonance for evaluation of mitral regurgitation prior to mitral valve surgery. J Thorac Dis 2017;9(Suppl 4):S246–S256.
35. Guo YK, Yang ZG, Ning G, et al. Isolated mitral regurgitation: quantitative assessment with 64-section multidetector CT—comparison with MR imaging and echocardiography. Radiology 2009;252(2):369–376.
36. van Rosendael PJ, van Wijngaarden SE, Kamperidis V, et al. Integrated imaging of echocardiography and computed tomography to grade mitral regurgitation severity in patients undergoing transcatheter aortic valve implantation. Eur Heart J 2017;38(28):2221–2226.
37. La Canna G, Arendar I, Maisano F, et al. Real-time three-dimensional transesophageal echocardiography for assessment of mitral valve functional anatomy in patients with prolapse-related regurgitation. Am J Cardiol 2011;107(9):1365–1374.
38. Gabriel RS, Kerr AJ, Raffel OC, Stewart RA, Cowan BR, Occleshaw CJ. Mapping of mitral regurgitant defects by cardiovascular magnetic resonance in moderate or severe mitral regurgitation secondary to mitral valve prolapse. J Cardiovasc Magn Reson 2008;10(1,Lv):16.
39. Lancellotti P, Tribouilloy C, Hagendorff A, et al. Recommendations for the echocardiographic assessment of native valvular regurgitation: an executive summary from the European Association of Cardiovascular Imaging. Eur Heart J Cardiovasc Imaging 2013;14(7):611–644.
40. Binder RK, Webb JG, Willson AB, et al. The impact of integration of a multidetector computed tomography annulus area sizing algorithm on outcomes of transcatheter aortic valve replacement: a prospective, multicenter, controlled trial. J Am Coll Cardiol 2013;62(5):431–438.
41. Guerrero M, Dvir D, Himbert D, et al. Transcatheter mitral valve replacement in native mitral valve disease with severe mitral annular calcification: results from the first multicenter global registry. JACC Cardiovasc Interv 2016;9(13):1361–1371.
42. Abdul-Jawad Altisent O, Dumont E, Dagenais F, et al. Initial experience of transcatheter mitral valve replacement with a novel transcatheter mitral valve: procedural and 6-month follow-up results. J Am Coll Cardiol 2015;66(9):1011–1019.
43. Cheung A, Webb J, Verheye S, et al. Short-term results of transapical transcatheter mitral valve implantation for mitral regurgitation. J Am Coll Cardiol 2014;64(17):1814–1819.
44. Muller DW, Farivar RS, Jansz P, et al. Transcatheter mitral valve replacement for patients with symptomatic mitral regurgitation: a global feasibility trial. J Am Coll Cardiol 2017;69(4):381–391.
45. Blanke P, Dvir D, Cheung A, et al. A simplified D-shaped model of the mitral annulus to facilitate CT-based sizing before transcatheter mitral valve implantation. J Cardiovasc Comput Tomogr 2014;8(6):459–467.
46. Naoum C, Leipsic J, Cheung A, et al. Mitral annular dimensions and geometry in patients with functional mitral regurgitation and mitral valve prolapse: implications for transcatheter mitral valve implantation. JACC Cardiovasc Imaging 2016;9(3):269–280.
47. Achenbach S, Delgado V, Hausleiter J, Schoenhagen P, Min JK, Leipsic JA. SCCT expert consensus document on computed tomography imaging before transcatheter aortic valve implantation (TAVI)/transcatheter aortic valve replacement (TAVR). J Cardiovasc Comput Tomogr 2012;6(6):366–380.
48. Mak GJ, Blanke P, Ong K, et al. Three-dimensional echocardiography compared with computed tomography to determine mitral nnulus size before transcatheter mitral valve implantation. Circ Cardiovasc Imaging 2016;9(6):e004176.
49. Clavel MA, Mantovani F, Malouf J, et al. Dynamic phenotypes of degenerative myxomatous mitral valve disease: quantitative 3-dimensional echocardiographic study. Circ Cardiovasc Imaging 2015;8(5):e002989.
50. Grewal J, Suri R, Mankad S, et al. Mitral annular dynamics in myxomatous valve disease: new insights with real-time 3-dimensional echocardiography. Circulation 2010;121(12):1423–1431.
51. Pressman GS, Movva R, Topilsky Y, et al. Mitral annular dynamics in mitral annular calcification: a three-dimensional imaging Study. J Am Soc Echocardiogr 2015;28(7):786–794.
52. Eleid MF, Cabalka AK, Williams MR, et al. Percutaneous transvenous transseptal transcatheter valve implantation in failed bioprosthetic mitral valves, ring annuloplasty, and severe mitral annular calcification. JACC Cardiovasc Interv 2016;9(11):1161–1174.
53. Yoon SH, Whisenant BK, Bleiziffer S, et al. Transcatheter mitral valve replacement for degenerated bioprosthetic valves and failed annuloplasty rings. J Am Coll Cardiol 2017;70(9):1121–1131.
54. Blanke P, Naoum C, Dvir D, et al. Predicting LVOT obstruction in transcatheter mitral valve implantation: concept of the Neo-LVOT. JACC Cardiovasc Imaging 2017;10(4):482–485.
55. Wang DD, Eng M, Greenbaum A, et al. Predicting LVOT obstruction after TMVR. JACC Cardiovasc Imaging 2016;9(11):1349–1352.
56. Qin JX, Shiota T, Lever HM, et al. Impact of left ventricular outflow tract area on systolic outflow velocity in hypertrophic cardiomyopathy: a real-time three-dimensional echocardiographic study. J Am Coll Cardiol 2002;39(2):308–314.
57. Kim DH, Handschumacher MD, Levine RA, et al. In vivo measurement of mitral leaflet surface area and subvalvular geometry in patients with asymmetrical septal hypertrophy: insights into the mechanism of outflow tract obstruction. Circulation 2010;122(13):1298–1307.
58. Blanke P, Dvir D, Naoum C, et al. Prediction of fluoroscopic angulation and coronary sinus location by CT in the context of transcatheter mitral valve implantation. J Cardiovasc Comput Tomogr 2015;9(3):183–192.
59. Thériault-Lauzier P, Dorfmeister M, Mylotte D, et al. Quantitative multi-slice computed tomography assessment of the mitral valvular complex for transcatheter mitral valve interventions. II. Geometrical measurements in patients with functional mitral regurgitation. EuroIntervention 2016;12(8):e1021–e1030.
60. Thériault-Lauzier P, Andalib A, Martucci G, et al. Fluoroscopic anatomy of left-sided heart structures for transcatheter interventions: insight from multislice computed tomography. JACC Cardiovasc Interv 2014;7(9):947–957.
61. Blanke P, Park JK, Grayburn P, et al. Left ventricular access point determination for a coaxial approach to the mitral annular landing zone in transcatheter mitral valve replacement. J Cardiovasc Comput Tomogr 2017;11(4):281–287.
62. Wunderlich NC, Siegel RJ. Peri-interventional echo assessment for the MitraClip procedure. Eur Heart J Cardiovasc Imaging 2013;14(10):935–949.
63. Lang RM, Badano LP, Mor-Avi V, et al. Recommendations for cardiac chamber quantification by echocardiography in adults: an update from the American Society of Echocardiography and the European Association of Cardiovascular Imaging. Eur Heart J Cardiovasc Imaging 2015;16(3):233–270.
64. Le Tourneau T, Deswarte G, Lamblin N, et al. Right ventricular systolic function in organic mitral regurgitation: impact of biventricular impairment. Circulation 2013;127(15):1597–1608.
65. Wasmer K, Zellerhoff S, Köbe J, et al. Incidence and management of inadvertent puncture and sheath placement in the aorta during attempted transseptal puncture. Europace 2017;19(3):447–457.
66. Wunderlich NC, Beigel R, Siegel RJ. The role of echocardiography during mitral valve percutaneous interventions. Cardiol Clin 2013;31(2):237–270.